Proceedings of the ASME 2010 3rd Joint US-European Fluids Engineering Summer Meeting and 8th International Conference on Nanochannels, Microchannels, and Minichannels
FEDSM-ICNMM2010
August 1-5, 2010, Montreal, Canada

FEDSM-ICNMM2010-30096

EFFECT OF MASS RATIO ON THE VORTEX-INDUCED VIBRATIONS OF A LONG TENSIONED BEAM IN SHEAR FLOW

Rémi Bourguet*
Massachusetts Institute of Technology
Cambridge, MA 02139, USA
Email: bourguet@mit.edu

Didier Lucor
Institut Jean le Rond d'Alembert
Paris, 75252, France
Email: didier.lucor@upmc.fr

Michael S. Triantafyllou
Massachusetts Institute of Technology
Cambridge, MA 02139, USA
Email: mistetri@mit.edu

ABSTRACT

The flow past a cylindrical tensioned beam of aspect ratio 200 *is predicted by direct numerical simulation of the three-dimensional Navier-Stokes equations. The beam is free to oscillate in inline and crossflow directions and submitted to a linearly sheared oncoming flow. The ratio between high and low inflow velocities is* 3.67*, with a maximum Reynolds number of* 330*. Two structure/fluid mass ratios are considered,* 6 *and* 3*. Structure vortex-induced vibrations are characterized by mixed standing-traveling wave patterns. A reduction of mass ratio from* 6 *to* 3 *leads to purer, more pronounced traveling wave responses and larger amplitude vibrations in both directions. While multifrequency structure vibrations are observed at* $m = 6$*, case* $m = 3$ *exhibits monofrequency responses. A large zone of synchronization between vortex shedding and structure vibration (lock-in) is identified in the high velocity region. The topology of fluid-structure energy exchanges shows that the flow can excite the structure at lock-in and damps its vibrations in non-lock-in region. Inline/crossflow motion synchronization is monitored. Similar zigzagging patterns of inline/crossflow motion phase difference are put forward for both mass ratios, highlighting a predominant character of counterclockwise orbits in the excitation region.*

INTRODUCTION

Vortex-Induced Vibrations (VIV) of long flexible structures are an important issue in the domain of applications and especially in the context of ocean engineering where a reliable estimation of fatigue damage implies an efficient prediction of this phenomenon. Several experimental works have emphasized the high physical complexity of this fluid-structure interaction problem, even in the idealized case of an elastically mounted rigid cylinder, as reviewed in Bearman (1984); Sarpkaya (2004); Williamson & Govardhan (2004).

The present numerical study focuses on the VIV of a long cylindrical tensioned beam free to oscillate in inline and crossflow directions in a linear shear flow, during the transition to turbulence. The objectives of this work are to quantify the influence of structure/fluid mass ratio on the nature of structure response and to examine its effects on lock-in phenomenon and fluid-structure energy exchanges.

Previous experimental studies concerning flexible cylinders in shear flow have underlined the possible occurrence of vibrations at a single or multiple frequencies (e.g. Kim *et al.*, 1986; Vandiver *et al.*, 1996; Trim *et al.*, 2005). In this physical context, structure responses characterized by mixed standing-traveling wave patterns have been reported (Lucor *et al.*, 2006; Vandiver *et al.*, 2009). The influence of the shear rate of the oncoming flow on lock-in has been emphasized by Vandiver *et al.* (1996). It has been shown in particular that strong shear can inhibit lock-in at multiple frequencies. The importance of the mass ratio on VIV phenomenon has been highlighted by Govardhan & Williamson (2002) in the case of an elastically mounted rigid cylinder, concerning especially the bandwidth of lock-in. In the present study, the influence of the mass ratio is investigated in the case of a flexible cylinder in shear flow with an emphasis on its effects

*Address all correspondence to this author.

on the above mentioned standing-traveling wave pattern and on mono-/multifrequency response development.

The physical model and numerical method are briefly described in the two first sections. The influence of mass ratio on structure response is examined in a third section and this analysis is related to fluid-structure interaction considerations in a fourth section. The main findings of this study are summarized in a fifth section.

PHYSICAL MODEL

The flow past a flexible cylinder is predicted by direct numerical simulation of the three-dimensional Navier-Stokes equations under incompressibility assumption. The structure is submitted to a crossflow parallel to x axis and linearly sheared along its span (z axis) as illustrated in figure 1. All physical variables are non-dimensionalized using the cylinder diameter D and the maximum inflow velocity U, located at $z = 0$. These reference quantities are used to define the Reynolds number. The ratio between maximum and minimum inflow velocity is 3.67. The local Reynolds number (Re) ranges from 330 to 90. The cylinder aspect ratio is $L/D = 200$, where L is its length in equilibrium position. The shear rate can be defined by $\beta = (D/U_m)\partial u/\partial z$ where U_m is mean oncoming flow velocity and u the local component of flow velocity parallel to x axis, $\beta = 0.0062$ in the present case. The cylinder is pinned at both ends and free to move in-between in x and y directions referred to as *inline* and *crossflow* directions in the following. The structure dynamics is governed by a tensioned beam model that can be expressed as follows in the non-dimensional formulation proposed by Evangelinos & Karniadakis (1999):

$$\frac{\partial^2 \zeta}{\delta t^2} - \omega_c^2 \frac{\partial^2 \zeta}{\delta z^2} + \omega_b^2 \frac{\partial^4 \zeta}{\delta z^4} + \frac{K}{m}\frac{\partial \zeta}{\delta t} = \frac{1}{2}\frac{C}{m}, \qquad (1)$$

where $\zeta = [\zeta_x, \zeta_y]^T$ with ζ_x and ζ_y, the inline and crossflow displacements of the cylinder, and $C = [C_x, C_y]^T$, with C_x and C_y the total drag and lift coefficients including both pressure and viscous contributions. t denotes time variable. The mass ratio is defined by $m = \rho_c/\rho_f D^2$ where ρ_c is the cylinder density per unit length and ρ_f the fluid density. It quantifies the cylinder mass over the displaced fluid mass. Two mass ratios, 6 and 3, are considered in this study. ω_c and ω_b are associated with the cable and beam terms and defined by $\omega_c^2 = T/m$ and $\omega_b^2 = EI/m$. T and EI are the constant non-dimensional tension and bending stiffness of the structure, ω_c and ω_b are also non-dimensional. A tensioned beam with $\omega_c = 4.55$ and $\omega_b = 9.09$ is considered. As shown in the following, these structural parameters lead to vibrations involving high structural modes representative of realistic configurations similar to the experimental study of Trim *et al.* (2005). The structural damping is neglected ($K = 0$) to allow maximum amplitude oscillations.

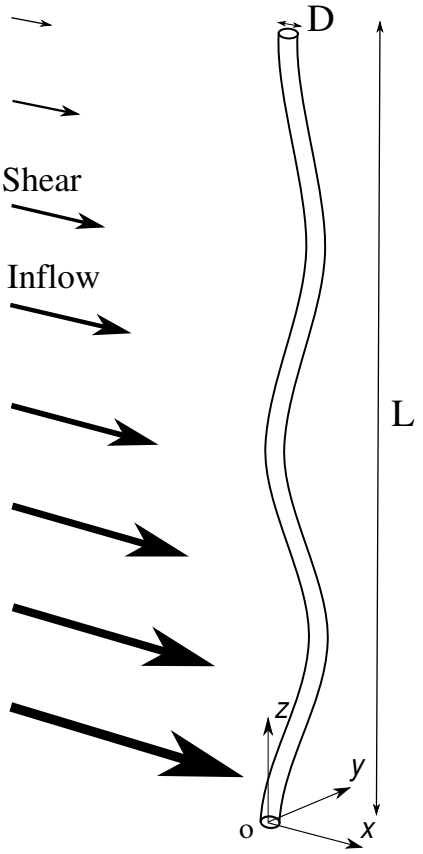

FIGURE 1. SKETCH OF THE PHYSICAL CONFIGURATION.

NUMERICAL METHOD

The coupled fluid-structure system is solved by the parallel code Nektar that is based on the spectral/hp element method (Karniadakis & Sherwin, 2005). This version of the code employs a hybrid scheme with Fourier expansion in spanwise z direction and Jacobi-Galerkin formulation on (x,y) planes. A boundary-fitted coordinate formulation is used to take into account the cylinder unsteady deformation. Details regarding time integration schemes and validation studies of the numerical method and parameters have been reported in Newman & Karniadakis (1997); Evangelinos & Karniadakis (1999) concerning similar physical configurations. The computational domain extends $50D$ downstream and $20D$ in front, above and below the cylinder. A two-dimensional grid of 2175 elements with polynomial order $p = 7$ is used on (x,y) planes. In z direction, 1024 planes (512 complex Fourier modes) are used. Fourier expansion implies spanwise periodicity of the flow and structure variables and of the imposed shear velocity profile. The technique sug-

gested by Lucor (2004) is adopted here. A buffer region of 8% of the cylinder length (16D) where the inflow velocity profile is adjusted to respect periodicity is considered in agreement with the recommendations of Lucor *et al.* (2006). The buffer region is not presented in the following. Numerical tests concerning the boundary conditions, computational domain and buffer region sizes have been performed in the above mentioned studies.

The analysis reported in this study is based on the monitoring of time series of more than 300 convective time units ($t^\star U/D$ with $t^\star$ the dimensional time variable) once the permanent regime is reached, with a non-dimensional sampling frequency equal to 40.

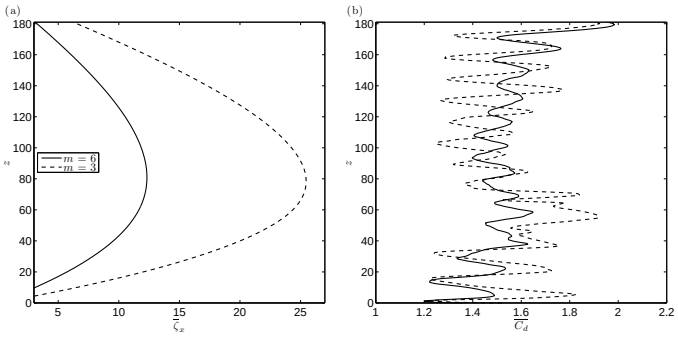

FIGURE 2. TIME-AVERAGED (a) INLINE DISPLACEMENT AND (b) DRAG COEFFICIENT ALONG CYLINDER SPAN.

STRUCTURE VIBRATIONS

The effect of mass ratio on structure vibrations is examined in this section. Spatio-temporal evolutions of inline and crossflow cylinder displacements are quantified and a spectral analysis is provided to identify the influence of mass ratio on the nature of structure response. Finally, the synchronization of inline and crossflow vibrations is studied with a special attention paid to the fundamental features persisting as mass ratio changes.

Time-averaged inline bending

The time-averaged inline displacement of the cylinder is presented in Fig. 2 as well as the time-averaged drag coefficient. In this plot, the drag is normalized by the local oncoming flow velocity. As expected from expression (1), cylinder bending increases as mass ratio is reduced. In both cases, the cylinder exhibits an asymmetric deformation due to shear flow, with a maximum displacement located near $z = 80$. Such asymmetric deformation has been observed experimentally by Chaplin *et al.* (2005) for a cylinder submitted to a stepped current, for example. Structure inline bending modifies the oncoming flow velocity normal to the cylinder. More precisely, for $z \in [0,80]$ approximately, the relative weight of the velocity component normal to the cylinder increases as z increases, opposing the effect of shear flow. For $z > 80$, structure bending can reinforce the effect of shear flow by reducing the component normal to the cylinder as z increases. The mean drag coefficient presents larger spatial fluctuations at $m = 3$. A larger spatial average of this coefficient in region $z \in [0,80]$ ($z > 80$) is observed at $m = 3$ ($m = 6$ respectively). The spatial evolution of the mean drag coefficient is strongly influenced by the structure response discussed in the following.

Spatio-temporal patterns

Selected time series of inline and crossflow displacements are presented along cylinder span in Fig. 3 and 4, once the permanent regime of the coupled fluid-structure system is reached. In these plots the temporal fluctuation of inline motion $\tilde{\zeta}_x$ about its mean deformation is considered. From a general and qualitative point of view, structure responses are characterized by a mixed combination of standing and traveling waves. The traveling character of the vibrations seems more pronounced in inline direction and preferentially oriented from high oncoming flow velocity region to low velocity region (increasing z). A strong standing wave character dominates the region near $z = 0$ in both directions and for both mass ratios until approximately $z = 40$.

It can be observed that in inline direction, this standing wave pattern is reinforced in this region at $m = 3$, which can be related to the above mentioned increased inline bending of the cylinder (Fig. 2 (a)). Beyond this region, stronger traveling wave responses develop. Reducing the mass ratio leads to purer traveling wave responses. This point is examined quantitatively in the following. It should be noticed that at $m = 6$, structure reponses exhibit significant temporal irregularities that almost vanish at $m = 3$. This is related to the occurrence of multifrequency vibrations as discussed in next section.

Statistics

Maximum and Root Mean Square (RMS) values of the displacements along cylinder span are plotted in Fig. 5. The influence of the standing wave character of structure responses is visible in all cases as illustrated by the alternance of nodes and anti-nodes. However, the fact that RMS values of displacements at nodes are not zero emphasizes the effect of traveling wave pattern. Except in the first spanwise cell, it appears that anti-node amplitudes remain relatively constant along cylinder span, in spite of the shear flow.

The reduction of mass ratio from 6 to 3 leads to larger vibration amplitudes in both directions in average (RMS values). The maximum amplitudes of crossflow vibrations are however very close which illustrates the irregular character of structure response at $m = 6$. In addition, it is interesting to notice that amplitudes between adjacent node and anti-node is generally smaller at $m = 6$. Successive changes of predominant excited structural mode in this case are responsible for this phenomenon as detailed

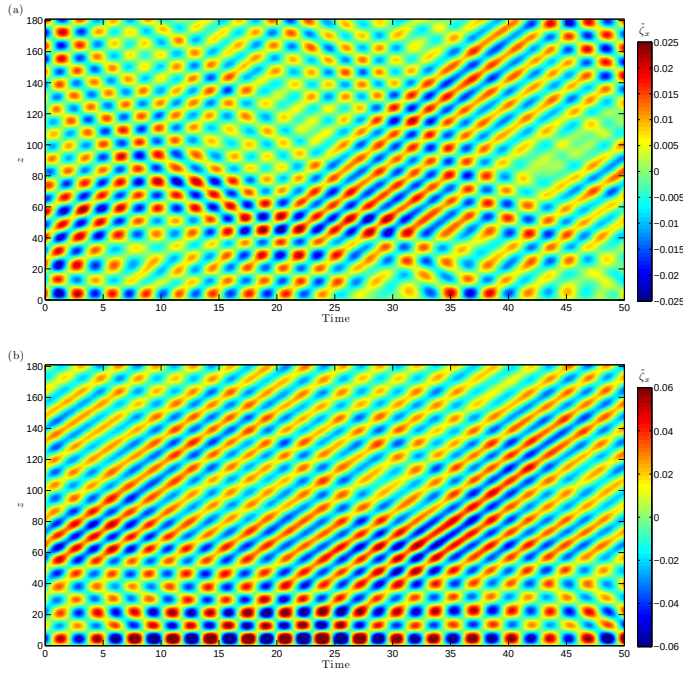

FIGURE 3. TEMPORAL EVOLUTION OF INLINE DISPLACEMENT FLUCTUATION ALONG CYLINDER SPAN FOR (a) $m = 6$ AND (b) $m = 3$.

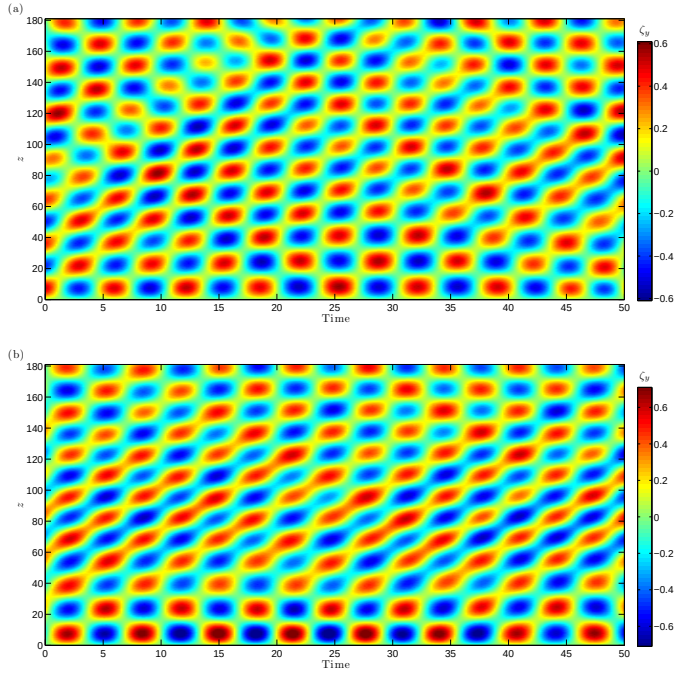

FIGURE 4. TEMPORAL EVOLUTION OF CROSSFLOW DISPLACEMENT ALONG CYLINDER SPAN FOR (a) $m = 6$ AND (b) $m = 3$.

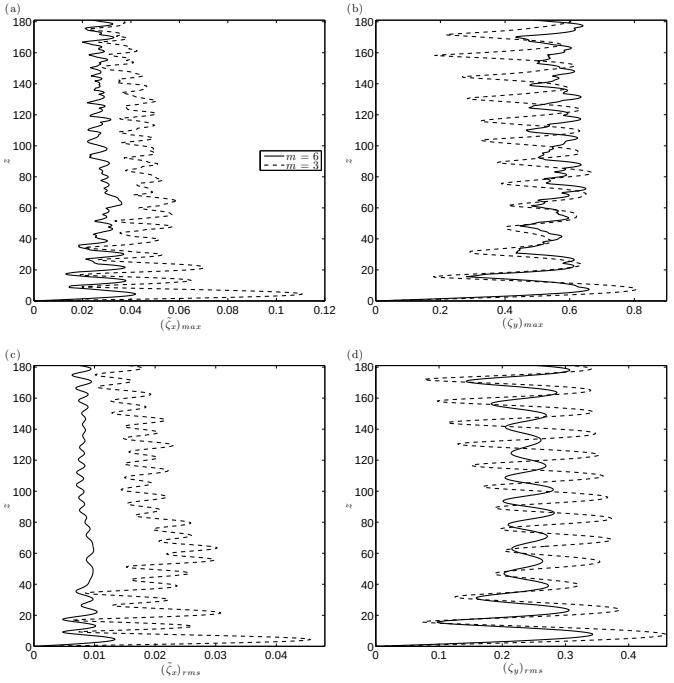

FIGURE 5. (a,b) MAXIMUM AMPLITUDE AND (c,d) RMS VALUE OF (a,c) INLINE DISPLACEMENT FLUCTUATION AND (b,d) CROSSFLOW DISPLACEMENT ALONG CYLINDER SPAN.

in the following on the basis of spectral analysis.

Spectral analysis

Spatio-temporal spectral analysis is carried out to clarify the nature of structure vibrations and the influence of mass ratio. This is achieved by a two-dimensional FFT of the spatio-temporal evolution of structure responses which are zero padded to reach a frequency resolution of 5×10^{-4} in both time and space. In Fig. 6, Power Spectral Densities (PSD) of inline and crossflow motions are plotted as functions of frequency and spatial wavenumber. Positive frequencies are presented and thus negative wavenumbers (upper part of each plot) are associated with traveling waves moving towards low velocity region while positive wavenumbers (lower part of each plot) represent traveling moving towards high velocity region. PSD are normalized by the maximum observed on both domains (positive and negative wavenumbers) to illustrate the traveling or standing character of the response. Sine Fourier modes ($\sin(\pi nzD/L)$ for the n^{th} mode) are often used to describe structure response (e.g. Chaplin *et al.*, 2005; Lie & Kaasen, 2006). The discretization of structure variables is based on this decomposition in the present numerical method (Evangelinos & Karniadakis, 1999) and thus it seems natural to associated the predominant spatial wavenumbers with the corresponding sine modes. Selected sine Fourier modes are indicated by white

horizontal dashed lines in Fig. 6.

From a general point of view a fundamental difference between the two configurations is that multifrequency responses are observed in both directions at $m = 6$ while case $m = 3$ exhibits monofrequency responses. Predominant excited modes correspond to $n \in \{22, 23, 24, 25\}$ in inline direction and $n \in \{13, 14, 15\}$ in crossflow direction at $m = 6$ and $n = 24$ in inline direction and $n = 14$ in crossflow direction at $m = 3$. These mode numbers are close to those measured experimentally by Trim *et al.* (2005) and Lie & Kaasen (2006), where cases of multi-frequency responses have been reported in shear flow.

At a given vibration frequency it appears that only one peak emerges on spatial spectrum at the same wavenumber on both negative and positive sides, i.e. only one structural mode is excited at a given frequency. The natural frequency f_n^{nat} of the tensioned beam associated with the n^{th} structural mode can be evaluated as follows, in vacuum:

$$f_n^{\text{nat}} = \frac{k_n}{2\pi}\sqrt{\omega_c^2 + \omega_b^2 k_n^2}, \quad \text{with} \quad k_n = \frac{\pi n D}{L}. \tag{2}$$

This spectrum can be modified to take into account of the immersion of the cylinder into the fluid:

$$f_n^{\text{mod}} = f_n^{\text{nat}}\sqrt{\frac{m}{m + \frac{\pi}{4}C_m}}, \tag{3}$$

where C_m is the added mass coefficient induced by the flow. In the absence of dynamical effects C_m is equal to 1. The corresponding modified frequencies are indicated by red crosses in Fig. 6. While this modified spectrum seems to provide a reasonable approximation of the effective excited frequencies in some cases, significant discrepancies appear in other cases emphasizing the strong influence of dynamical effects.

The relative weights of negative and positive wavenumber peaks for the same frequency provide information concerning the standing/traveling character of the corresponding mode. In all cases, negative peak dominate, denoting predominant traveling wake moving from high velicty region to low velocity region (increasing z). It can be observed that the ratio between negative and positive peak amplitudes for a given frequency is generally larger at $m = 3$. This is in agreement with the previous remark concerning the occurrence of purer, reinforced traveling waves at $m = 3$.

As a first step, vibrations have been investigated independently in each direction. The synchronization between inline and crossflow motions is studied in next section.

Inline/crossflow synchronization

Recently, Vandiver *et al.* (2009) and Modarres-Sadeghi *et al.* (2010) have emphasized, on the basis of experimental measurements involving flexible cylinders in shear flows, a possible link between inline/crossflow motion synchronization and the distribution of excitation and damping regions along the span. This link is examined here with an emphasis on mass ratio effect.

The instantaneous phases of inline and crossflow vibrations (ϕ_x and ϕ_y respectively) are determined by means of Hilbert transform. Adopting an approach similar to Huera-Huarte & Bearman (2009), the phase difference Φ_{xy} is evaluated as follows:

$$\Phi_{xy} = [p\phi_x - q\phi_y, \quad \text{mod } 360^o], \tag{4}$$

where p and q are two integer numbers defining the level of synchronization studied. Considering the conclusions of the previous spectral analysis, the couple $(p,q) = (1,2)$ is chosen here. Values of Φ_{xy} in the range $0^o - 180^o$ ($180^o - 360^o$ respectively) correspond to "figure eight" orbits where the cylinder moves upstream (dowstream respectively) when reaching crossflow oscillation maxima. These two types of trajectories are referred to as *counterclockwise* and *clockwise* respectively, as suggested by Dahl *et al.* (2007).

Histograms of Φ_{xy} are evaluated from the whole vibration time series. Figure 7 shows at each spanwise location, the relative weights of phase difference angles. The contributions are normalized by the maximum weight. A predominant phase difference can be clearly identified in most cases.

The main effect induced by mass ratio modification is related to the mono- or multifrequency character of the vibrations: case $m = 6$ exhibits a noisier phase difference pattern since multimoded responses occur in both directions, with possible synchronization lag. However, spanwise distribution of phase difference presents strong similarities in both cases and is characterized by a zigzagging pattern drifting regularly towards high phase angles as z increases. In case of pure standing waves, a discontinuous phase difference with regular jumps between clockwise and counterclockwise orbits would be observed while a case of pure traveling waves could exhibit constant phase difference. The above mentioned zizagging pattern is a composition of these two idealized cases. The fact that counterclockwise motion dominates the high velocity region for the two studied mass ratios is in agreement with the experimental observations of Modarres-Sadeghi *et al.* (2010).

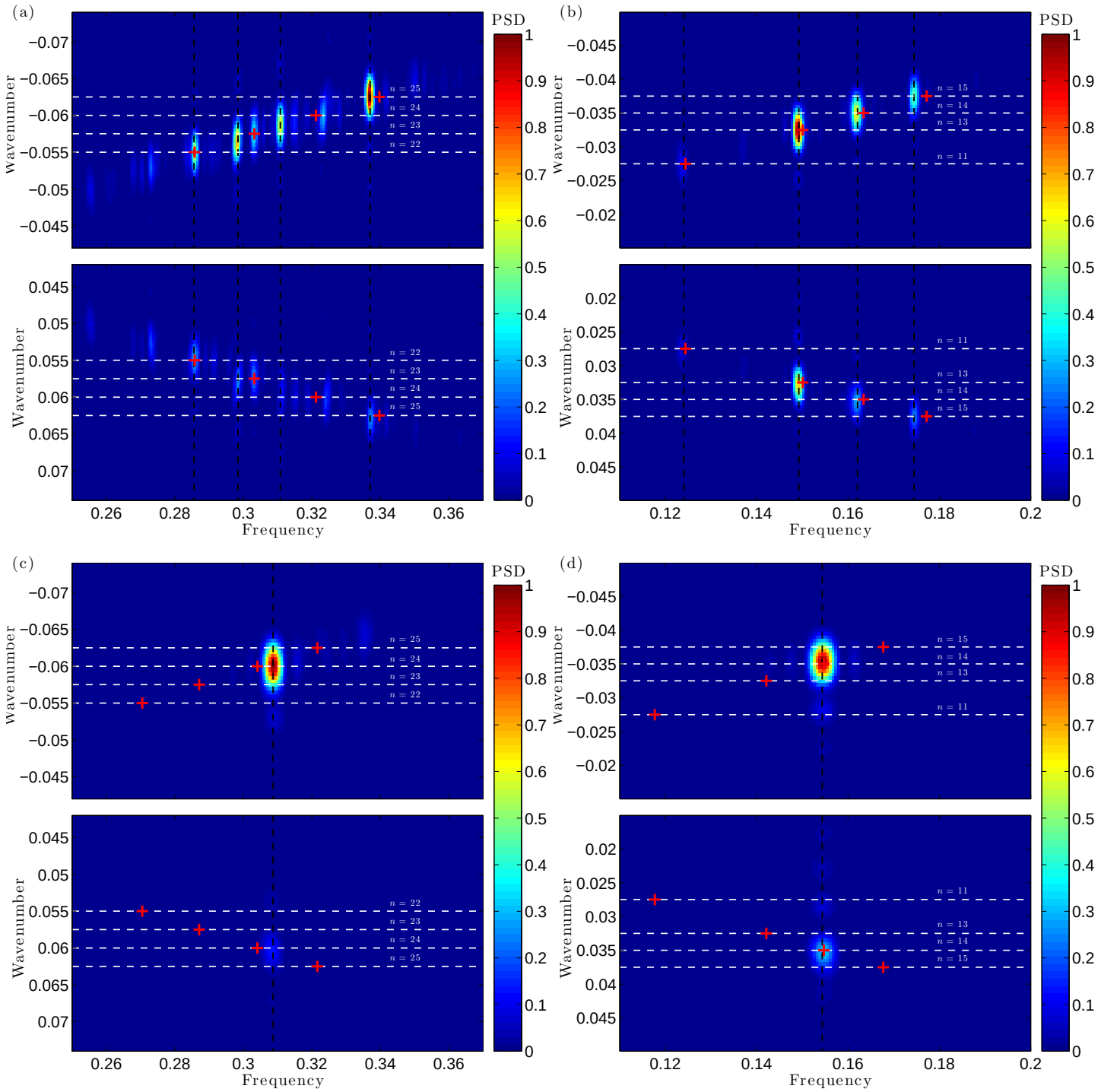

FIGURE 6. SPATIO-TEMPORAL SPECTRAL ANALYSIS OF (a,c) INLINE DISPLACEMENT FLUCTUATION AND (b,d) CROSSFLOW DISPLACEMENT FOR (a,b) $m = 6$ AND (c,d) $m = 3$. BLACK VERTICAL DASHED LINES INDICATE PREDOMINANT FREQUENCIES. WAVENUMBERS OF SELECTED SINE FOURIER MODES ARE INDICATED BY WHITE HORIZONTAL DASHED LINES. RED CROSSES DENOTE THE MODIFIED FREQUENCIES OF THESE MODES.

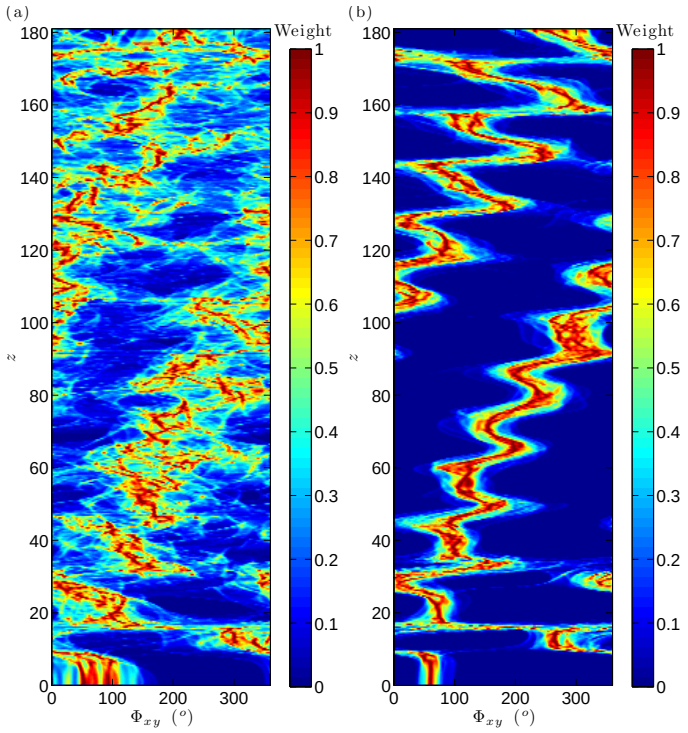

FIGURE 7. HISTOGRAM OF INLINE/CROSSFLOW MOTION PHASE DIFFERENCE ALONG CYLINDER SPAN FOR (a) $m = 6$ AND (b) $m = 3$.

FLUID-STRUCTURE INTERACTION

This section focuses on the influence of mass ratio on the coupled fluid-structure system. The phenomenon of lock-in in shear flow is examined with an emphasis on lock-in/non-lock-in distribution along cylinder span, before analyzing the topology of fluid-structure energy exchanges.

Lock-in

The present linear shear flow can potentially excite broad band response spectra since the natural vortex shedding frequency depends on the oncoming velocity. In the case of forced crossflow oscillations of rigid and flexible cylinders in shear flow, Stansby (1976) and Peltzer & Rooney (1985) have emphasized the formation of long ($> 40D$) spanwise cells of constant shedding frequency equal to forcing frequency. Lock-in phenomenon consists in a synchronization between vortex shedding and structure oscillation. The partial lock-in of the wake reported in previous references perturbs the pattern observed in the case of stationary cylinders in shear flow (or stationary tapered cylinders in uniform flow) that is composed of smaller cells of constant shedding frequency separated by regular discontinuities (Noack *et al.*, 1991).

Crossflow component of flow velocity v has been recorded over the same time interval as structure displacements along a spanwise line downstream of the cylinder at $(x,y) = (20,0)$ in case $m = 6$ and $(x,y) = (31,0)$ in case $m = 3$. PSD of v temporal evolution is plotted along the span in Fig. 8. Selected frequencies previously identified by spectral analysis of structure vibrations (Fig. 6) are indicated by dashed lines.

Two main spanwise regions can be distinguished in both cases. A zone of lock-in can be identified in the high velocity region, near $z = 0$. The rest of the span corresponds to non-lock-in region where vortex shedding and structure vibrations are not synchronized. At $m = 6$, lock-in occurs at the three frequencies associated with the predominant modes of crossflow vibration while case $m = 3$ exhibits lock-in at a single frequency. Lock-in occurs over $75D$ at $m = 6$ and $77D$ at $m = 3$. However, within high-velocity region, zones exist where no peak can be clearly identified, leading to spatial intermittencies of lock-in. At lock-in, shedding frequency can be driven relatively far from the natural shedding frequency past a stationary cylinder. Shedding frequencies normalized by the local oncoming flow velocity are in the ranges $[0.149, 0.213]$ and $[0.154, 0.222]$ at $m = 6$ and $m = 3$ respectively.

Non-lock-in region is characterized by a cellular pattern relatively similar to the case of a stationary cylinder in shear flow as reported in (Peltzer & Rooney, 1985) with a comparable shear rate. The wake pattern (not presented here) is characterized by oblique vortex shedding that are responsible for the preferential orientation of the traveling wave responses. To satisfy the continuity of spanwise vortex filaments while vortex shedding freqiency is discontinuous, vortex splitting events (e.g. Williamson, 1992; Piccirillo & Van Atta, 1993; Zhang *et al.*, 1995) occur at the boundaries of each spanwise cell in Fig. 8.

Energy exchanges

Fluid-structure energy exchanges are quantified in average by means of the lift coefficient in phase with structure crossflow velocity:

$$C_{lv}(z) = \frac{\frac{2}{T_s}\int_{T_s} C_y(z,t)\dot{\zeta}_y(z,t)dt}{\sqrt{\frac{2}{T_s}\int_{T_s}\dot{\zeta}_y^2(z,t)dt}}, \qquad (5)$$

where T_s is the sampling period. The present analysis focuses on crossflow displacements since the structure mainly vibrates in this direction.

Spanwise evolution of C_{lv} is plotted in Fig. 9 for both cases. Zones of positive C_{lv} are located in the high velocity region and coincide with lock-in regions. In regions where vortex shedding

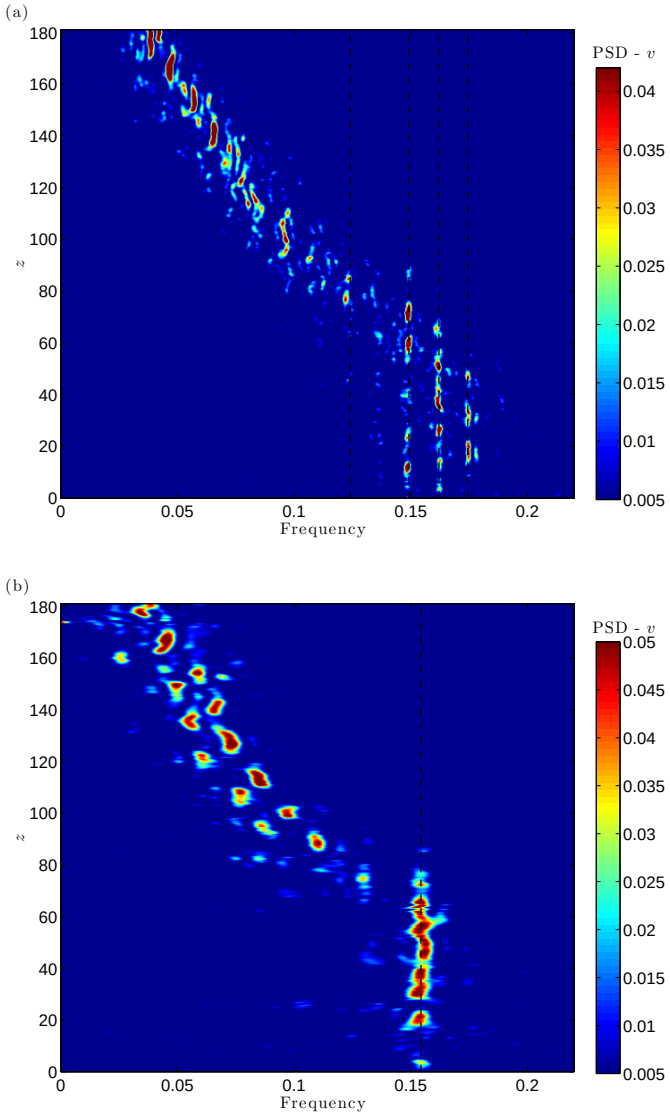

FIGURE 8. PSD OF THE TEMPORAL EVOLUTION OF CROSS-FLOW COMPONENT OF FLOW VELOCITY ALONG A SPANWISE LINE AT (a) $(x,y) = (20,0)$, $m = 6$ AND (b) $(x,y) = (31,0)$, $m = 3$. DASHED LINES INDICATE PREDOMINANT FREQUENCIES OF STRUCTURE VIBRATION.

and structure oscillation are not synchronized, C_{lv} remains negative. As a consequence, the flow can excite the structure at lock-in ($C_{lv} > 0$) whereas its damps structure oscillations elsewhere ($C_{lv} < 0$). C_{lv} exhibits strong irregularities in lock-in region in both cases and its spanwise pattern is more regular out of lock-in region, where it is negative. It can be noticed that in excitation region, counterclockwise orbits dominate the synchronization pattern between inline and crossflow vibrations (Fig. 7).

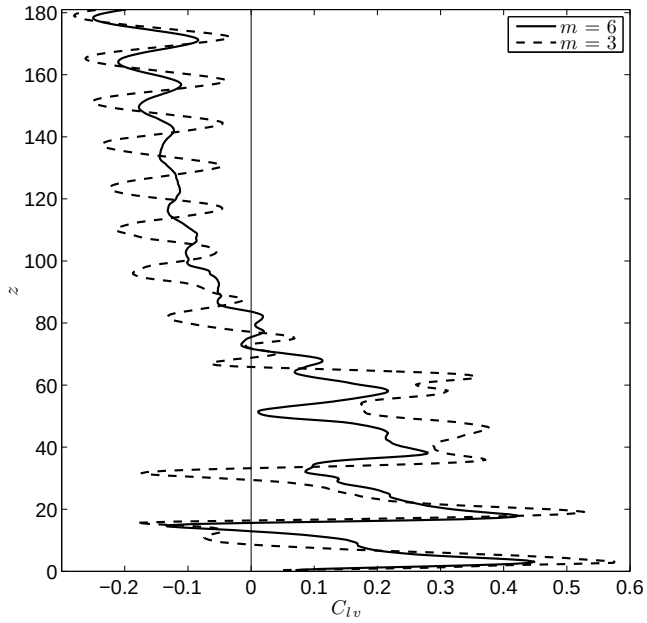

FIGURE 9. LIFT COEFFICIENT IN PHASE WITH VELOCITY ALONG CYLINDER SPAN.

Some differences related to mass ratio modification can be underlined in this region. The reinforced standing wave pattern near the end ($z < 40$) at $m = 3$, because of the increased bending of the structure, induces stronger modulations of C_{lv} that becomes negative near crossflow vibration nodes. Beyond this region, where a purer traveling wave response develops ($z \in [40,68]$), C_{lv} reaches higher values with reduced spanwise variations at $m = 3$.

SUMMARY

The coupled fluid-structure system composed of a long flexible cylinder in shear flow has been simulated at a Reynolds number ranging from 330 to 90.

Structure response is characterized by a mixed standing-traveling wave pattern. The influence of cylinder mass ratio on structure response has been investigated. A reduction of mass ratio from 6 to 3 leads to larger amplitude vibrations and purer responses: purer standing waves for $z < 40$ and purer, more pronounced traveling waves beyond this region. While multi-frequency structure vibrations are observed in both directions at $m = 6$, case $m = 3$ exhibits monofrequency responses.

Spanwise extent of lock-in region is similar for both cases: vortex shedding and structure oscillation remain synchronized over more than $75D$. The fundamental features of inline/crossflow motion synchronization are not altered by the

passage from multifrequency to monofrequency reponses: the phase difference between inline and crossflow motions exhibits a zigzagging pattern along cylinder span and counterclockwise orbits dominate high velocity excitation region in both cases. This could emphasize a relative generality of this synchronization pattern for flexible cylinders in shear flow, that is corroborated by experimental observations as mentioned previously.

ACKNOWLEDGMENT

Financial support was provided by the BP-MIT Major Projects Program, and BP America Production Co.

REFERENCES

Bearman, P. W. 1984 Vortex shedding from oscillating bluff bodies. *Annual Review of Fluid Mechanics* **16**, 195–222.

Chaplin, J. R., Bearman, P. W., Huera-Huarte, F. J. & Pattenden, R. J. 2005 Laboratory measurements of vortex-induced vibrations of a vertical tension riser in a stepped current. *Journal of Fluids and Structures* **21**, 3–24.

Dahl, J. M., Hover, F. S., Triantafyllou, M. S., Dong, S. & Karniadakis, G. E. 2007 Resonant vibrations of bluff bodies cause multivortex shedding and high frequency forces. *Physical review letter* **99**, 144503.

Evangelinos, C. & Karniadakis, G. E. 1999 Dynamics and flow structures in the turbulent wake of rigid and flexible cylinders subject to vortex-induced vibrations. *Journal of Fluid Mechanics* **400**, 91–124.

Govardhan, R. & Williamson, C. H. K. 2002 Resonance forever: existence of a critical mass and an infinite regime of resonance in vortexinduced vibration. *Journal of Fluid Mechanics* **473**, 147–166.

Huera-Huarte, F. J. & Bearman, P. W. 2009 Wake structures and vortex-induced vibrations of a long flexible cylinder part 1: Dynamic response. *Journal of Fluids and Structures* **25**, 969–990.

Karniadakis, G. E. & Sherwin, S. 2005 *Spectral/hp Element Methods for CFD*. Oxford: Oxford University Press.

Kim, Y. H., Vandiver, J. K. & Holler, R. 1986 Vortex-induced vibration and drag coefficients of long cables subjected to sheared flow. *ASME Journal of Energy Resources Technology* **108**, 77–83.

Lie, H. & Kaasen, K. E. 2006 Modal analysis of measurements from a large-scale viv model test of a riser in linearly sheared flow. *Journal of Fluids and Structures* **22**, 557–575.

Lucor, D. 2004 Generalized polynomial chaos: applications to random oscillators and flow-structure interactions. PhD Thesis, Brown University.

Lucor, D., Mukundan, H. & Triantafyllou, M. S. 2006 Riser modal identification in CFD and full-scale experiments. *Journal of Fluids and Structures* **22**, 905–917.

Modarres-Sadeghi, Y., Mukundan, H., Dahl, J. M., Hover, F. S. & Triantafyllou, M. S. 2010 The effect of higher harmonic forces on fatigue life of marine risers. *Journal of Sound and Vibration* **329**, 43–55.

Newman, D. J. & Karniadakis, G. E. 1997 A direct numerical simulation study of flow past a freely vibrating cable. *Journal of Fluid Mechanics* **344**, 95–136.

Noack, B. R., Ohle, F. & Eckelmann, H. 1991 On cell formation in vortex streets. *Journal of Fluid Mechanics* **227**, 293–308.

Peltzer, R. D. & Rooney, D. M. 1985 Vortex shedding in a linear shear flow from a vibrating marine cable with attached bluff bodies. *Journal of Fluids Engineering* **107**, 61–66.

Piccirillo, P. S. & Van Atta, C. W. 1993 An experimental study of vortex shedding behind linearly tapered cylinders at low reynolds number. *Journal of Fluid Mechanics* **246**, 163–195.

Sarpkaya, T. 2004 A critical review of the intrinsic nature of vortex-induced vibrations. *Journal of Fluids and Structures* **19**, 389–447.

Stansby, P. K. 1976 The locking-on of vortex shedding due to the cross-stream vibration of circular cylinders in uniform and shear flows. *Journal of Fluid Mechanics* **74**, 641–665.

Trim, A. D., Braaten, H., Lie, H. & Tognarelli, M. A. 2005 Experimental investigation of vortex-induced vibration of long marine risers. *Journal of Fluids and Structures* **21**, 335–361.

Vandiver, J. K., Allen, D. & Li, L. 1996 The occurrence of lock-in under highly sheared conditions. *Journal of Fluids and Structures* **10**, 555–561.

Vandiver, J. K., Jaiswal, V. & Jhingran, V. 2009 Insights on vortex-induced, traveling waves on long risers. *Journal of Fluids and Structures* **25**, 641–653.

Williamson, C. H. K. 1992 The natural and forced formation of spot-like 'vortex dislocations' in the transition of a wake. *Journal of Fluid Mechanics* **243**, 393–441.

Williamson, C. H. K. & Govardhan, R. 2004 Vortex-induced vibrations. *Annual Review of Fluid Mechanics* **36**, 413–455.

Zhang, H.-Q., Fey, U., Noack, B. R., Konig, M. & Eckelmann, H. 1995 On the transition of the cylinder wake. *Physics of Fluids* **7**, 779–794.